MNRAS 000, 1–8 (2018) Preprint 2 May 2018 Compiled using MNRAS LATEX style file v3.0

Multi-phase outflows as probes of AGN accretion history

Emanuele Nardini[1⋆] and Kastytis Zubovas[2,3]
[1] *INAF – Osservatorio Astrofisico di Arcetri, Largo Enrico Fermi 5, I-50125 Firenze, Italy*
[2] *Center for Physical Sciences and Technology, Saulėtekio av. 3, Vilnius LT-10257, Lithuania*
[3] *Vilnius University Observatory, Saulėtekio av. 9, Bldg III, Vilnius LT-10222, Lithuania*

Released Xxxx Xxxxx XX

ABSTRACT
Powerful outflows with a broad range of properties (such as velocity, ionization, radial scale and mass loss rate) represent a key feature of active galactic nuclei (AGN), even more so since they have been simultaneously revealed also in individual objects. Here we revisit in a simple analytical framework the recent remarkable cases of two ultraluminous infrared quasars, IRAS F11119+3257 and Mrk 231, which allow us to investigate the physical connection between multi-phase AGN outflows across the ladder of distance from the central supermassive black hole (SMBH). We argue that any major deviations from the standard outflow propagation models might encode unique information on the past SMBH accretion history, and briefly discuss how this could help address some controversial aspects of the current picture of AGN feedback.

Key words: galaxies: active – galaxies: evolution – quasars: general – quasars: supermassive black holes – ISM: jets and outflows

1 INTRODUCTION

The past few years have witnessed a rapid progress in the detection and characterization of outflow signatures in active galactic nuclei (AGN), also thanks to the development of new powerful techniques based on interferometry and integral field spectroscopy. In the most luminous objects at any redshift, the inferred mass and momentum rates of the outflowing gas are much larger than the star formation rate of the host galaxy and the momentum rate of the AGN radiation field, respectively (e.g. Maiolino et al. 2012; Rupke & Veilleux 2013; Liu et al. 2013; Cicone et al. 2014; Carniani et al. 2015; Bischetti et al. 2017; González-Alfonso et al. 2017). Outflows of this kind are therefore the best candidates for the widely invoked feedback agency that solves several open issues with galaxy evolution models (Kormendy & Ho 2013, and references therein), bridging the small and the large scales by returning to the host galaxy a significant fraction of the energy released during the growth of the central supermassive black hole (SMBH). The actual impact of AGN-driven outflows on the ability of the host systems to sustain their star formation activity, however, is still unclear, as the observable effects depend on a number of factors, such as sample selection, adopted diagnostics and temporal delays, thus delivering controversial indications (see Harrison 2017 for a recent review, and references therein).

Despite these uncertainties, the mounting evidence for galaxy-wide molecular outflows apparently complying with the adiabatic expansion of hot bubbles inflated by ultra-fast, accretion-disc winds (e.g. Tombesi et al. 2015) represents a potential breakthrough in many respects. The coexistence of multiple outflow flavours in individual objects is definitely intriguing, but at the same it poses some interpretational challenges. In fact, it is not obvious that the evolution of a SMBH wind can be tracked simultaneously at various stages in a single source, as some of these are arguably short-lived (at least in terms of detectability). If anything, the different response times to changes in the AGN activity level will reduce the probability that simultaneity also implies causal connection. The optimal conditions for the launch of high-velocity, high-column density X-ray winds, for instance, are met at the highest accretion rates (King & Pounds 2003; Takeuchi, Ohsuga & Mineshige 2013), close to or exceeding the Eddington limit, which cannot be preserved over periods comparable to the entire outflow lifetimes, which are typically of several million years. Moreover, while the emission signatures of neutral outflowing gas can still be visible at the largest scales a long time after the driving AGN episode has faded (King, Zubovas & Power 2011), absorption and highly ionized features are unlikely to be detached from the parent activity spell. Numerical simulations (Gabor & Bournaud 2014), as well as empirical (Schawinski et al. 2015) and theoretical arguments (King & Nixon 2015), suggest that AGN have a flickering behaviour, with bursts as short as $\sim 10^5$ yr. A slowly fading AGN luminosity after such Eddington-limited 'flares' would still correlate with the outflow properties on kpc scales (Zubovas 2018), possibly alleviating but not completely solving the time-scale issues.

⋆ E-mail: enardini@arcetri.astro.it

In this paper, we revisit some of the most recent findings on multi-phase AGN outflows, discussing not only their implications in the context of the driving mechanism and propagation through the host galaxy, but also the potential application of outflows as a powerful means of probing the accretion history of the SMBH itself. Over the lifetime of a galaxy, a flickering AGN can generate an 'outflow cascade' that will expand into an ever different medium, especially in chaotic accretion (Nayakshin, Power & King 2012) and merger scenarios (Capelo et al. 2015). What we observe today might then be the compound of several previous events of highly efficient accretion. The prospect of disentangling the nuclear activity history by inspecting the properties of multi-phase outflows foreshadows novel insights into the way galaxies are shaped by their central engines.

2 UNIFICATION OF AGN OUTFLOWS

Most AGN exhibit some kind of outflow signatures, which, depending on their exact nature, might arise over a wide range of distances from the nucleus. Mildly relativistic winds pervading the SMBH neighbourhood are identified through blueshifted absorption lines from highly ionized iron in the hard X-ray spectra (Tombesi et al. 2010), and are regarded as the ultimate trigger for AGN feedback (e.g. Nardini et al. 2015). Moving towards larger radii (and lower ionization states), the most prevalent outflow tracers materialize as soft X-ray and ultraviolet (UV) warm absorbers (Crenshaw & Kraemer 2012), UV broad absorption lines (BALs; Gibson et al. 2009), blue wings in the optical absorption (Rupke & Veilleux 2011) and emission lines (Harrison et al. 2014), molecular P-Cygni profiles in the far-infrared (Sturm et al. 2011) and broad, spatially resolved emission lines in the sub-millimetric (Feruglio et al. 2010). In some of these cases, the typical ranges of both distance and velocity partly overlap. For the sake of simplicity, throughout this paper we use the terms 'wind' and 'outflow' to describe, respectively, the faster/inner phases and the slower/outer ones.

Whether these disparate outflow manifestations, often characteristic of AGN with different luminosities, redshifts and host-galaxy properties, can be considered as consecutive snapshots of the same process is far from straightforward. At least in the quasar luminosity regime ($L_{\rm bol} \sim 10^{46}$ erg s^{-1}), the compilation of X-ray winds and molecular outflows from the literature is compatible with the predictions of inefficient cooling of the shocked gas (Zubovas & King 2012; Faucher-Giguère & Quataert 2012). Yet, uncertainties and systematics are extremely large, and still not compensated for by sufficient sample statistics. The recent study by Fiore et al. (2017) has confirmed a strong correlation between the properties of each outflow flavour (including also [O III], BALs and warm absorbers) and AGN luminosity, but the connection between the various phases remains unclear (see their Fig. 2). The key physical parameters of two coexisting X-ray and molecular components were first measured by Tombesi et al. (2015), who discovered strongly blueshifted Fe K absorption in IRAS F11119+3257, an ultraluminous infrared galaxy (ULIRG) already known to host a massive OH outflow (Veilleux et al. 2013b). The relation between Fe K and OH energetics was suggested to support the scenario of an energy-conserving flow. This case is re-examined below, together with another remarkable example that became available soon afterwards, Mrk 231 (Feruglio et al. 2015).

2.1 Mass outflow rates

In order to maximize the information that can be extracted from the comparison of different phases, we need to accurately assess the amount of energy carried outwards by the accretion-disc wind in the first place. Here we compute the initial mass outflow rate through the expression:

$$\dot{\mathcal{M}}_{\rm wind} \simeq \Omega N_{\rm H} m_{\rm p} \mathcal{V} \mathcal{R}, \tag{1}$$

implicitly assuming solar abundances, full ionization, and neglecting any more complex geometrical dependence with no significant loss of accuracy (e.g. Krongold et al. 2007). In Eq. (1), $m_{\rm p}$ is the proton mass, Ω is the solid angle subtended by the wind, and $N_{\rm H}$, $\mathcal{V}$ and $\mathcal{R}$ are its column density, velocity and inner radius. As, with very few exceptions, solid angle and starting point cannot be properly constrained from the X-ray spectrum, we adopt $\Omega_{\rm FeK}/4\pi = 0.5$ (Nardini et al. 2015) and $\mathcal{R}_{\rm FeK} = 2c^2/\mathcal{V}^2_{\rm FeK}$ (i.e., the escape radius in units of gravitational radii, $r_{\rm g} = GM_{\rm BH}/c^2$), so that:

$$\dot{\mathcal{M}}_{\rm FeK} \simeq 9.4\, N_{24} M_8 \beta^{-1} \times 10^{24}\ {\rm g\ s^{-1}}, \tag{2}$$

where N_{24} is the column density in units of 10^{24} cm^{-2}, M_8 is the SMBH mass in units of $10^8\, M_\odot$, and $\beta = \mathcal{V}_{\rm FeK}/c$. This is roughly equivalent to $0.15\, N_{24} M_8 \beta^{-1}\ M_\odot\ {\rm yr^{-1}}$.

The mass outflow rate of the large-scale components is instead averaged over their flow time, $\dot{\mathcal{M}}_{\rm out} = \mathcal{M}\mathcal{V}\mathcal{R}^{-1}$, as this is more appropriate for the comparison with a global outflow dynamics powered by a single AGN episode of constant luminosity. Hence, for the molecular gas phases, it is:

$$\dot{\mathcal{M}}_{\rm out} \simeq 6.5\, \mathcal{M}_8 \mathcal{V}_3 \mathcal{R}^{-1}_{\rm kpc} \times 10^{27}\ {\rm g\ s^{-1}}, \tag{3}$$

where $\mathcal{M}_8$ is the total outflowing mass in $10^8\, M_\odot$, $\mathcal{V}_3$ is the velocity in 10^3 km s^{-1}, $\mathcal{R}_{\rm kpc}$ is the distance in kpc, and the numerical factor is about 100 $M_\odot$ yr^{-1}. A 'fiducial' radius is frequently used in Eq. (3), yet here we consistently identify $\mathcal{R}_{\rm kpc}$ with the smallest spatial scale affected by the outflow. The meaning of $\mathcal{R}$ in Eqs. (1–3) thus implies that our estimates of $\dot{\mathcal{M}}$ and of its dependent quantities should be treated as lower/upper limits for the wind/outflow cases. The motivations behind this conservative choice will become clearer in Section 3, once all the relevant pieces of information on the sources under examination are in hand.

2.2 Black hole masses

To begin with, it is immediately evident from Eq. (2) that a reliable estimate of the SMBH mass is very important. This also controls another crucial ingredient of our analysis, the Eddington ratio: the lower the mass, the higher the (average) accretion rate the AGN has to maintain to drive an outflow towards the edge of the galaxy. The values of M_8 reported in the literature for both IRAS F11119+3257 and Mrk 231 span more than an order of magnitude. We therefore resort to the latest scaling relations between virial radius of the broad line region and black hole mass (Bentz et al. 2013), and apply them to the de-reddened optical spectra of Zheng et al. (2002; see their discussion of the correction

for extinction local to the source). For a full width at half-maximum (FWHM) of the Hβ line of $\sim$2000 km s^{-1}, intrinsic $\lambda L_\lambda(5100\,\text{Å}) \simeq 12.1\,L_\odot$, and virial coefficient $f = 1$, we evaluate a SMBH mass in IRAS F11119+3257 of $M_8 = 1.95^{+0.80}_{-0.54}$ (see also Hao et al. 2005). Note that the most recent works on this object have used an appreciably smaller value ($M_8 = 0.16$, after Kawakatu, Imanishi & Nagao 2007), which, however, turns out to be underestimated by a factor of $\sim$5 (N. Kawakatu, private communication).

For Mrk 231, exhibiting a FWHM (Hβ) $\simeq$ 3100 km s^{-1} and an extinction-corrected $\lambda L_\lambda(5100\,\text{Å}) \simeq 11.5\,L_\odot$, we find $M_8 = 2.40^{+0.55}_{-0.40}$. This is remarkably similar to the mass inferred by Leighly et al. (2014) employing the Paα line width and the 1 μm continuum luminosity (following Landt et al. 2013). Considerably lower and fairly higher values are returned, respectively, by the correlations with the stellar velocity dispersion from CO 1.6 μm ro-vibrational band heads ($M_8 = 0.17$; Dasyra et al. 2006) and with the H-band magnitude of the host spheroid ($M_8 = 3.8$; Veilleux et al. 2009a). Yet, the former method is known to yield systematically small velocity dispersions (e.g. Rothberg et al. 2013), while the latter, in these hybrid, IR-bright systems, might suffer from heavy starburst contamination. Consequently, the corresponding dynamical and photometric black hole masses are most likely extremes, and are deemed to be less reliable than the virial ones we have retrieved above.

2.3 IRAS F11119+3257

As previously mentioned, the unexpected detection of an ultra-fast wind in IRAS F11119+3257 has opened unprecedented perspectives. Since minor variations between different epochs are negligible for our purposes, the gas velocity, $\beta = 0.253^{+0.061}_{-0.118}$, and column density, $N_{24} = 3.2\,(\pm1.5)$, are derived from a follow-up observation of the source performed with *NuSTAR* (Tombesi et al. 2017), which samples the continuum also beyond the Fe K absorption feature and so provides tighter constraints on its position (β) and depth (N_{24}). By using these values and $M_8 = 1.95$ in Eq. (2), we obtain mass and momentum rates for the X-ray wind of $\dot{\mathcal{M}}_{\rm FeK} \sim 1.5$–$6.5\ M_\odot$ yr^{-1} and $\dot{\mathcal{P}}_{\rm FeK} = \dot{\mathcal{M}}_{\rm FeK}\mathcal{V}_{\rm FeK} \sim 0.8$–$2.8 \times 10^{36}$ dyne. It is worth noting that the latter, under our prescription for $\mathcal{R}_{\rm FeK}$, does not explicitly depend on β.

The properties of the OH 119 μm outflow were determined by Tombesi et al. (2015) through the radiative transfer model described in González-Alfonso et al. (2014), for a relative OH abundance of 2.5×10^{-6}. The absorbing material was constrained to lie within 0.1–1.0 kpc from the SMBH, with $\mathcal{V}_{\rm OH} \simeq 1000\,(\pm200)$ km s^{-1}. Based on our assumptions, we get $\dot{\mathcal{M}}_{\rm OH} \sim 200$–$1500\ M_\odot$ yr^{-1} and $\dot{\mathcal{P}}_{\rm OH} \sim 1$–$9 \times 10^{36}$ dyne. Subsequent ALMA observations have also revealed broad wings (with nominal velocity $\mathcal{V}_{\rm CO} = 1000$ km s^{-1}) in the CO (1–0) emission line profile, spatially extended over distances of $\sim$4–15 kpc (Veilleux et al. 2017). The standard conversion factor of 0.8 between CO line luminosity and total molecular (H_2) mass in ULIRGs (Downes & Solomon 1998) delivers $\mathcal{M}_8 \sim 10\,(\pm4)$, hence $\dot{\mathcal{M}}_{\rm CO} \sim 140$–$370\ M_\odot$ yr^{-1} and $\dot{\mathcal{P}}_{\rm CO} \sim 0.7$–$2.5 \times 10^{36}$ dyne. The values of all the quantities of interest are summarized in Table 1.

The three main outflow flavours in IRAS F11119+3257, Fe K, OH and CO, are reported as red points in the momentum rate versus velocity diagram of Fig. 1, with no further corrections. Notably, evidence for widespread outflows in this source is also found in other gas phases, in particular Na I D (Rupke, Veilleux & Sanders 2005), [O III] (Lípari et al. 2003) and [Ne V] (Spoon & Holt 2009), but unfortunately none of these has been investigated as yet in sufficient detail to be assigned a precise location in this plot.

Table 1. AGN and outflow properties in IRAS F11119+3257 and Mrk 231. $\dot{M}_{\rm A}$ is the mass accretion rate, α the relative AGN contribution to the bolometric luminosity ($L_{\rm bol}$), and η the SMBH radiative efficiency. Note that the values provided for each outflow rate (mass, momentum, energy) neglect systematic uncertainties, and are meant to represent either lower (Fe K, BAL) or upper (OH, CO) limits (see the text for the full set of assumptions). OH entries for Mrk 231 refer to the high-velocity components from González-Alfonso et al. (2017), corrected to match our criteria.

	IR 11119	Mrk 231
$\log(M_{\rm BH}/M_\odot)$	8.29 ± 0.15	8.38 ± 0.09
$\log(L_{\rm bol}/L_\odot)$	12.67	12.60
$L_{\rm AGN}/L_{\rm Edd}$	0.73α	0.50α
$\dot{M}_{\rm A}$ ($M_\odot$ yr^{-1})	$0.31\alpha\eta^{-1}$	$0.27\alpha\eta^{-1}$
$\dot{\mathcal{M}}_{\rm FeK}$ ($M_\odot$ yr^{-1})	$3.6^{+2.9}_{-2.1}$	$1.4^{+2.0}_{-0.8}$
$\dot{\mathcal{P}}_{\rm FeK}$ ($L_{\rm bol}/c$)	$2.9^{+1.9}_{-1.6}$	$0.36^{+0.48}_{-0.21}$
$\dot{\mathcal{E}}_{\rm FeK}$ ($L_{\rm bol}$)	$0.37^{+0.25}_{-0.27}$	$0.012^{+0.016}_{-0.007}$
$\dot{\mathcal{M}}_{\rm BAL}$ ($M_\odot$ yr^{-1})	–	12^{+8}_{-4}
$\dot{\mathcal{P}}_{\rm BAL}$ ($L_{\rm bol}/c$)	–	$0.67^{+0.50}_{-0.32}$
$\dot{\mathcal{E}}_{\rm BAL}$ ($L_{\rm bol}$)	–	$0.005^{+0.005}_{-0.003}$
$\dot{\mathcal{M}}_{\rm OH}$ ($M_\odot$ yr^{-1})	600^{+900}_{-400}	(1370)
$\dot{\mathcal{P}}_{\rm OH}$ ($L_{\rm bol}/c$)	$6.4^{+9.6}_{-4.5}$	(11.0)
$\dot{\mathcal{E}}_{\rm OH}$ ($L_{\rm bol}$)	$0.011^{+0.017}_{-0.009}$	(0.012)
$\dot{\mathcal{M}}_{\rm CO}$ ($M_\odot$ yr^{-1})	255 ± 115	870 ± 330
$\dot{\mathcal{P}}_{\rm CO}$ ($L_{\rm bol}/c$)	2.7 ± 1.5	9.2 ± 4.5
$\dot{\mathcal{E}}_{\rm CO}$ ($L_{\rm bol}$)	$0.005^{+0.003}_{-0.004}$	0.013 ± 0.008

2.4 Mrk 231

Being an AGN-dominated ULIRG, Mrk 231 qualifies as the nearest quasar known. Given its proximity and excellent observational coverage, it is the ideal target to explore all the possible connections between AGN-driven outflows. Indeed, Mrk 231 displays almost every kind of outflow features commonly found among AGN (e.g. Lípari et al. 2009; Feruglio et al. 2010; Fischer et al. 2010; Rupke & Veilleux 2011; González-Alfonso et al. 2014; Aalto et al. 2015; Morganti et al. 2016). A very deep *Chandra* exposure in the X-rays has recently brought out also a moderately fast Fe K wind ($\beta = 0.067^{+0.007}_{-0.010}$; Feruglio et al. 2015), whose properties are determined as above. With $N_{24} = 0.27^{+0.36}_{-0.15}$ and $M_8 = 2.4$, from Eq. (2) we now obtain $\dot{\mathcal{M}}_{\rm FeK} \sim 0.6$–$3.4\ M_\odot$ yr^{-1} and $\dot{\mathcal{P}}_{\rm FeK} \sim 0.7$–$4.3 \times 10^{35}$ dyne (Table 1).

Mrk 231 also belongs to the subclass of FeLoBALs, in that it shows broad UV absorption in several transitions of low-ionization species, including Fe II. This allows us to probe an intermediate scale (in $\log \mathcal{R}$) between the accretion disc and the host galaxy. The location of the gas responsible for these features was estimated to be of the order of 0.1

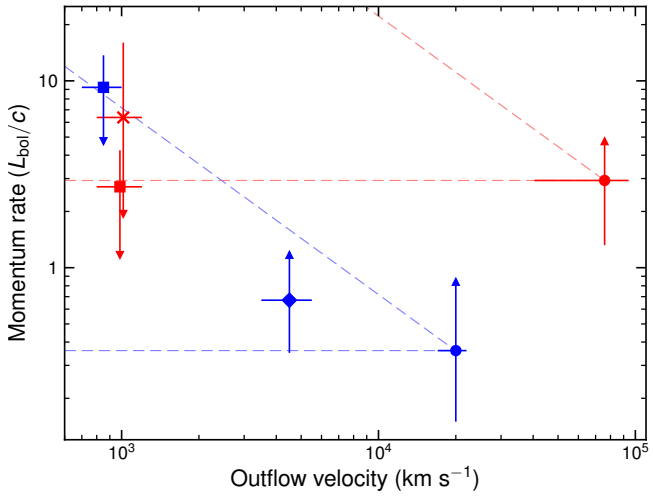

Figure 1. Momentum rate (in units of $L_{\rm bol}/c$) against velocity of the multi-phase outflows in IRAS F11119+3257 (red) and Mrk 231 (blue). The different symbols refer to the outflow type: Fe K (dot), BAL (diamond), OH (cross), and CO (square). The dashed horizontal and diagonal lines correspond to momentum and energy conservation. Error bars (1σ) are purely statistical, while arrows indicate whether a given measure should be considered as a lower or an upper limit (see the text for details).

kpc by Leighly et al. (2014), by applying a photoionization model, while Veilleux et al. (2016) argued for distances as small as a few pc, based on the physical conditions necessary to detect absorption from excited states of Fe II. The BAL mass ouflow rate is then calculated using Eq. (1), assuming a covering factor of $\Omega_{\rm BAL}/4\pi = 0.2$ (Dunn et al. 2010) and a radius of $\mathcal{R}_{\rm BAL} = 2$ pc. Accordingly, this should be taken as a conservative measure as well. For $\mathcal{V}_{\rm BAL} \sim 4500\,(\pm1000)$ km s^{-1} and $N_{24} \simeq 0.05^{+0.03}_{-0.01}$ (Leighly et al. 2014), we derive $\dot{\mathcal{M}}_{\rm BAL} \sim 8$–$20\ M_\odot$ yr^{-1} and $\dot{\mathcal{P}}_{\rm BAL} \sim 1.8$–$6 \times 10^{35}$ dyne.

We finally consider the CO (2–1) outflow from Feruglio et al. (2015). The mass outflow rate has some mild radial dependence out to $\sim$1.3 kpc, with nearly constant velocity, $\mathcal{V}_{\rm CO} \simeq 850\,(\pm150)$ km s^{-1}. Here we take into account the total mass, $\mathcal{M}_8 \simeq 3\,(\pm1)$, which has been corrected for the slightly larger CO-to-H_2 conversion factor used in this work. For $\mathcal{R}_{\rm CO} = 0.3$ kpc, the resulting mass and momentum rates are, respectively, $\dot{\mathcal{M}}_{\rm CO} \sim 540$–$1200\ M_\odot$ yr^{-1} and $\dot{\mathcal{P}}_{\rm CO} \sim 2.4$–$7 \times 10^{36}$ dyne. Feruglio et al. (2015) also showed that the neutral gas phase occupies a well-defined region of the momentum rate versus velocity diagram (Fig. 1), even when studied through alternative tracers. We can therefore take advantage of the wealth of available data on Mrk 231 to independently support the inferred outflow rates. By converting to our definitions the parameters of the two high-velocity ($\mathcal{V}_{\rm OH} = 550$ and 700 km s^{-1}) OH components identified by González-Alfonso et al. (2017), we indeed achieve fully consistent reference values, which are listed within brackets in Table 1. In the wake of this excellent match, in the remainder of this paper we can safely adopt our CO-based estimates as representative of the large-scale, neutral outflow.

3 DISCUSSION

The diagram in Fig. 1 has been mostly read so far as a diagnostic of the launching and driving mechanisms of AGN outflows. For this reason, the momentum rate is conveniently normalized to $L_{\rm AGN}/c$, giving the boost factor ($\mathcal{B}$) over the AGN radiative input. For a wind initially driven by radiation pressure in the Eddington regime, and then expanding adiabatically, the boost factor grows from $\mathcal{B} \sim 1$ at launch to $\mathcal{B} \sim$ 10–20 at kpc scales (Zubovas & King 2012). As ULIRGs are also host to fierce star formation, whose contribution to the total energy output is not trivial to disentangle from that of the AGN (e.g. Nardini et al. 2010), the measure of $L_{\rm AGN}$ is somewhat dependent on the adopted method. We thus prefer to normalize the momentum rates to $L_{\rm bol}/c$, where the bolometric luminosity is $L_{\rm bol} \sim 1.8$ and 1.5×10^{46} erg s^{-1} for IRAS F11119+3257 and Mrk 231, respectively (Veilleux et al. 2009b). This only introduces a common, minor (both sources are widely believed to be AGN-dominated) shift downwards of each point in the 'momentum boost' diagram of Fig. 1, without affecting their relative positions. Much larger uncertainties are associated to all the assumptions underlying our estimates, as emphasized earlier in our derivation of the mass (hence momentum) outflow rates. We refer to Harrison et al. (2018) for a more extensive discussion on these issues. Here we have resolved to partly keep the impact of systematics under control by not dealing with the 'actual' values of $\dot{\mathcal{P}}$, but with indicative lower (Fe K, BAL) and upper (OH, CO) limits.

In this context, we follow a simple analytical approach for the interpretation of Fig. 1, as this can be already very informative. At accretion rates close to Eddington, the wind's optical depth to electron scattering (τ) is naturally around unity (King & Pounds 2003; Reynolds 2012). Consequently, in the single-scattering limit, it is:

$$\dot{\mathcal{P}} = \dot{\mathcal{M}}\mathcal{V} \simeq \tau \frac{L_{\rm AGN}}{c} \sim \frac{L_{\rm AGN}}{c}. \tag{4}$$

If we now define $\dot{m}_{\rm A}$ and $\dot{m}_{\rm L}$ as the mass accretion and loss rates in units of Eddington, and η as the SMBH radiative efficiency, two immediate ramifications of Eq. (4) are:

$$\eta \simeq \frac{\dot{m}_{\rm L}}{\dot{m}_{\rm A}} \frac{\mathcal{V}}{c} = \frac{\dot{m}_{\rm L}}{\dot{m}_{\rm A}} \beta \tag{5}$$

and

$$\dot{\mathcal{E}} = \frac{1}{2}\dot{\mathcal{M}}\mathcal{V}^2 \simeq \frac{1}{2}\beta L_{\rm AGN}, \tag{6}$$

where $\dot{\mathcal{E}}$ is the rate at which mechanical energy is injected into the host environment through the fast X-ray wind. These approximations can be reasonably applied to both IRAS F11119+3257 and Mrk 231, for which $\dot{m}_{\rm A} \sim 0.7\alpha$ and 0.5α, respectively, where α is the fractional AGN contribution to $L_{\rm bol}$. Incidentally, we note that Eq. (5), with accurate data over large samples, could provide independent constraints on the SMBH spin distribution. Irrespective of the exact value of η, the range of $\dot{\mathcal{M}}_{\rm FeK}$ plainly encompasses also the mass accretion rate for both AGN (Table 1). Given the sizeable uncertainties, in the following we can assume $\dot{m}_{\rm L} \sim \dot{m}_{\rm A}$ with no loss of generality, so that $\eta = \beta$.

From Fig. 1, a striking contrast emerges between the various outflow manifestations in IRAS F11119+3257 (red) and in Mrk 231 (blue). In the former source, despite a difference in distance of at least an order of magnitude, the

OH and CO components have nearly identical velocity and very similar mass outflow rates, as if the outflow were not yet coasting but mass loading had stopped. Furthermore, both molecular phases lie rather far from the predictions for a fully energy-conserving case, based on the contemporary thrust of the Fe K wind. This, in particular, is apparently at odds with the claim of Tombesi et al. (2015), who used a finite thickness of the OH shell to compute an 'instantaneous' value of $\dot{\mathcal{P}}_{\rm OH}$, and corrected $\dot{\mathcal{P}}_{\rm FeK}$ downwards to match the inferred OH covering factor of $\sim$0.2. The properties in Fig. 1 would entail a stable energy input from the AGN over several Myr (see also Veilleux et al. 2017), but a fairly small coupling efficiency between the fast and the slow components. Alternatively, $\dot{\mathcal{P}}_{\rm FeK}$ must be either overestimated or higher than in past epochs. Yet, our revised measure of the SMBH mass does not require the SMBH to accrete at super-Eddington rates, so the present activity could have been maintained for a period commensurate with the age of the CO outflow ($\mathcal{R}_{\rm CO}/\mathcal{V}_{\rm CO} > 4$ Myr), especially in a ULIRG, where the gas supply to the central regions is governed by enhanced gravitational disturbances.

This notwithstanding, it should be kept in mind that in our analysis we are comparing truly 'instantaneous' (X-ray wind) and 'time-averaged' (molecular outflow) quantities, so the ratio $\mathcal{T}_{\rm FeK}^{\rm CO} = \mathcal{E}_{\rm CO}/\dot{\mathcal{E}}_{\rm FeK}$ represents an equally effective but less biased indicator to constrain the wind efficiency. The mechanical energy of the CO phase integrated over its flow time (which only depends on observables: total outflowing mass and velocity) is $\mathcal{E}_{\rm CO} \sim 0.4$–$1.6\times10^{58}$ erg, and it can be provided by the SMBH wind in just $\mathcal{T}_{\rm FeK}^{\rm CO} \sim 0.01$–$0.27$ Myr. This range can be stretched up to $0.4\alpha^{-1}$ Myr by directly using Eq. (6), but this would neglect the fact that $\dot{\mathcal{P}}_{\rm FeK}$ in IRAS F11119+3257 formally exceeds $L_{\rm AGN}/c$ by a factor of $\sim 3\alpha^{-1}$, consistent with the estimated optical depth of the wind, $\tau \geqslant 2.5$ ($N_{\rm H}$ is insensitive to any fully ionized gas). We thus conclude that $\mathcal{T}_{\rm FeK}^{\rm CO} \ll \mathcal{R}_{\rm CO}/\mathcal{V}_{\rm CO}$. Whether this is symptomatic of a real discrepancy between the energetics and lifetime of the CO outflow and the current AGN activity level is contingent upon the fraction of energy injected into the system through the fast wind that is eventually converted into bulk motion of the shocked ambient gas. This amount also depends on the density and metallicity of the interstellar medium (ISM), but it is typically of the order of $\sim$10–20 per cent of the input mechanical energy (e.g. Richings & Faucher-Giguère 2017). The range for $\mathcal{T}_{\rm FeK}^{\rm CO}$ above is therefore $\sim$5–10 times shorter than the intrinsic wind lifetime, $\mathcal{T}_{\rm wind}$. None the less, some tension remains, which can be further mitigated by allowing for a combination of narrower opening angle and iron overabundance (hence smaller equivalent $N_{\rm H}$), but is unlikely to be completely removed unless the source has also been caught in an unusual Fe K outburst state, implying a high degree of fine-tuning.

In this light, we cannot rule out the possibility that the CO outflow is actually the result of a previous Eddington-limited accretion episode. We follow this conjecture in the simplified analytical framework that describes the galactic environment as an isothermal sphere (e.g. Zubovas & King 2012), according to which the relation between mass outflow rate and velocity of the swept-up gas is given by:

$$\dot{\mathcal{M}} \simeq \frac{2f_{\rm g}\sigma^2}{G}\mathcal{V}, \tag{7}$$

where $f_{\rm g}$ is the gas fraction and σ is the velocity dispersion. The very presence of a large-scale outflow suggests that the SMBH in IRAS F11119+3257 has already reached the $M_{\rm BH}$–σ relation (King 2010), so we can assume $\sigma = 180$ km s^{-1} (as appropriate for $M_8 \sim 2$; Kormendy & Ho 2013) and apply Eq. (7) to the CO phase, deriving $f_{\rm CO} \sim 0.01$–0.025, which is much smaller than the cosmological value, $f_{\rm c} \simeq 0.16$. Were it still pushed by a constant driving force $L_{\rm AGN}/c$, such a tenuous gas component should travel at significantly larger velocity (King et al. 2011):

$$\mathcal{V} \simeq \frac{\gamma+1}{2}\left[\frac{2\eta\dot{m}_{\rm A}f_{\rm c}}{3f_{\rm g}}\sigma^2 c\right]^{1/3} \approx 3000 \text{ km s}^{-1}, \tag{8}$$

with γ specific heat ratio, $f_{\rm g} = f_{\rm CO}$ and $\eta\dot{m}_{\rm A} \sim \beta$ (Eq. 5). From this, as per equation (7) in Zubovas & King (2012), we can infer the radius ($R_{\rm off}$) where the putative coasting stage started, after a sudden AGN switch-off:

$$\left(\frac{\mathcal{V}_{\rm CO}}{V_{\rm off}}\right)^2 \sim 3\left(\frac{R_{\rm off}}{\mathcal{R}_{\rm CO}}\right)^2 - 2\left(\frac{R_{\rm off}}{\mathcal{R}_{\rm CO}}\right)^3. \tag{9}$$

In this scenario, the outflow must have lost radiative support when its distance from the AGN was about one fifth of the current one, which, for constant deceleration, corresponds to at least 1.5 Myr ago. This guess strongly depends on the actual radius of the CO shell, whose thickness of $\sim$10 kpc is indeed quite challenging, but widely separated AGN episodes are more likely to have distinct energy budgets (e.g. $\dot{\mathcal{E}}_{\rm FeK}$). We could argue that what we see on the large scales, although consistent with the steady driving from an AGN of lower, relatively constant luminosity (proportional to the duty cycle of Eddington-limited accretion; cf. Veilleux et al. 2017), is in fact the result of several short $\dot{m}_{\rm A} \sim 1$ bursts (e.g. Zubovas & King 2016), only entraining the diffuse ISM of the galaxy while leaving behind the denser clumps. Molecules can form at later times within the outflow (Zubovas & King 2014), as radiative cooling occurs within $\sim$1 Myr under most circumstances (Richings & Faucher-Giguère 2017). Projection effects, however, are certainly involved, and radial profiles of velocity and mass outflow rate would be needed to distinguish between different histories. It is also worth noting that, if multiple gas phases coexist at the same radius, the total mass outflow rate can be easily underestimated, and so the required duration of Eddington-limited AGN activity ($\sim\mathcal{T}_{\rm wind}$).

Turning now to the interpretation of the OH outflow in IRAS F11119+3257, this is exempt from the main shortcomings that affect its CO counterpart. The SMBH wind can take up to $\mathcal{T}_{\rm FeK}^{\rm OH} = \mathcal{E}_{\rm OH}/\dot{\mathcal{E}}_{\rm FeK} \sim 0.03$ Myr to supply the kinetic energy carried by the OH phase, $\mathcal{E}_{\rm OH} \sim 0.13$–$1.5\times10^{57}$ erg. Considering the amount of wind's mechanical power that ends up stored as thermal energy of the shocked ISM or used in the gravitational and expansion work, there is already overlap with the OH flow time of 0.1–1 Myr. Moreover, at sub-kpc scales inverse Compton cooling by the AGN radiation field can lead to non negligible radiative losses in the shocked wind (Ciotti & Ostriker 1997, 2001; King 2003). With no compelling necessity for the AGN to be more powerful than in the recent past, it is then plausible that the Fe K and OH flows are both part of the same AGN event, related to the ongoing luminous stage. Remarkably, this implies that even momentum boosts of a few ($\mathcal{B}_{\rm OH}/\mathcal{B}_{\rm FeK} \sim 2$) can be fully compatible with the adiabatic expansion of hot

wind bubbles. On the other hand, the similarity of the OH and CO outflow velocities might just be serendipitous, due to the fact that OH is driven to slower speeds because it is denser ($f_{\rm OH} \sim 0.01$–0.10 from Eq. 7), consistent with the hypothesis that some clumps survived the previous outflow(s) to be disrupted by the current one.

Based on Fig. 1, the outflows in Mrk 231 are apparently much easier to explain. This relies on two obvious reasons: the SMBH wind is about four times slower, and the outflow is extended only out to ~ 3 kpc (Rupke & Veilleux 2011). The mechanical energy of the molecular gas, $\mathcal{E}_{\rm CO} \sim 1.3$–$3 \times 10^{57}$ erg, can be released by the AGN in $\mathcal{T}_{\rm Fek}^{\rm CO} \sim 0.1$–$1.3$ Myr, in perfect agreement with the age of the outflow. As the three phases share a common range of kinetic power at ~ 0.5–$1 \alpha^{-1}$ per cent of $L_{\rm AGN}$ (Table 1), Mrk 231 seems, at face value, a genuine case of energy conservation. Once a realistic efficiency is taken into account, however, the Fe K wind is presumably too faint to propel the CO outflow, in spite of the lower/upper limit nature of their relative figures. In this sense, the BAL component would actually stand out as a more convincing driver, since its mass-loss rate can be substantially underestimated if our choice of $\mathcal{R}_{\rm BAL}$ is overly conservative. The most critical aspect is thus the physical relationship between the Fe K and BAL winds.

An X-ray/UV connection is well-established in AGN for the slower warm absorbers (Crenshaw & Kraemer 2012), where the various features arise in the same, stratified medium, yet Fe K absorption and BALs are rarely seen together. Consequently, their possible links have been never investigated in great detail, also because the initial conditions in numerical simulations of AGN outflows do not need to firmly discriminate between the two. While evidence for an intrinsic X-ray weakness of BAL quasars is now growing (e.g. Luo et al. 2014), with Mrk 231 itself fitting into this picture (Teng et al. 2014), the UV spectral properties of sources hosting ultra-fast X-ray winds have been largely overlooked so far. In Mrk 231, it would be tempting to speculate that we are witnessing, thanks to the X-ray weakness, the transition from continuum to line driving, as the ionization in the pre-shock SMBH wind drops with distance. This, however, is likely too simplistic once compared to the highly complex UV spectrum, which rather points to a clumpy outflow (Veilleux et al. 2013a, 2016). In general, Fe K and BAL features could even be co-spatial at sub-pc scales, if disc winds are strongly inhomogeneous (e.g. Hamann et al. 2018).

4 FUTURE DEVELOPMENTS

In this paper, we have illustrated how the 'momentum boost' diagram could become a powerful tool not only for attempting a connection between the different manifestations of outflows in AGN, but also for reconstructing an empirical history of SMBH accretion. Under the hypothesis of a virtually adiabatic expansion of the hot, shocked winds (Faucher-Giguère & Quataert 2012), the proposed application of this diagram is very promising, since any major deviations from the expected trends would then be directly attributable to fluctuations in the past AGN activity. Our re-examination of IRAS F11119+3257 and Mrk 231, carried out within a basic analytical framework and intended as a preliminary proof of concept, is still incapable of providing any conclusive results, owing to the large measure uncertainties and systematics. For these objects, however, there is ample room for cutting the error bars down through the acquisition of higher quality data, whereas filling the 'momentum boost' diagram with other outflow phases would allow a better sampling of the velocity and mass outflow rate radial profiles. Systematics can instead be overcome only through unbiased campaigns to increase the overall statistics, a step that is now widely recognized as mandatory (Cicone et al. 2018).

A complementary effort on the theoretical side is also desirable. Future observations should be complemented by more detailed simulations to take into account the time-evolution of AGN activity, wind mechanical power and ISM properties, with specific regard for the peculiar ULIRG environment. Indeed, ULIRGs might easily depart from the main assumptions of the current analytical models, such as spherical symmetry, and also the appropriateness of the standard SMBH scaling relations is somewhat questionable. Even so, ULIRGs remain the best laboratories to study AGN feedback in its radiative mode (Fabian et al. 2012). Finding the most powerful outflows in the local Universe among ULIRGs (e.g. González-Alfonso et al. 2017; Rupke, Gültekin & Veilleux 2017) is nothing but an indirect consequence of cosmic downsizing. It is not our aim here to discuss the global effects of AGN outflows, but it is not particularly surprising that their impact is rather limited in Seyfert galaxies (Bae et al. 2017; Rosario et al. 2018), where $\dot{m}_{\rm A} \sim 0.01$–$0.1$. In sub-Eddington AGN, continuum scattering is not an effective mechanism for driving persistent X-ray winds, which are then unlikely to deposit enough energy to sustain a feedback process as required by galaxy evolution models. This is reflected by a twofold observational evidence, for which not only are Fe K winds in Seyferts slower, on average, than in quasars ($\beta < 0.1$ against $\beta > 0.2$), but they also have a markedly transient nature. Their detection rate, in Seyferts with at least one such claim over multiple observations, is well below 50 per cent, with just a handful of exceptions (Tombesi et al. 2010; Gofford et al. 2013).

Conversely, ultra-fast winds are almost ubiquitous in the high-efficiency accretion regime of quasars, and likewise in that of Narrow-Line Seyfert 1 galaxies (Hagino et al. 2016; Parker et al. 2017) and ultraluminous X-ray sources (Pinto, Middleton & Fabian 2016). In ULIRGs, the merger-induced dissipation of ISM angular momentum and the subsequent availability of an abundant gas supply for SMBH growth can give rise to prolonged and/or recursive Eddington-limited accretion phases. In addition, also line driving and radiation pressure on dust (Ishibashi, Fabian & Maiolino 2018) can significantly contribute to push the wind outwards, making it possible in the long term to fully erode the dense cold clumps that would otherwise survive owing to Rayleigh-Taylor instabilities. Clumps might re-form further out, resulting in an inside-out quenching (Tacchella et al. 2015) and even in residual star formation (Maiolino et al. 2017).

The 'Eddington connection' between quasars/ULIRGs, Narrow-Line Seyfert 1 galaxies (NLS1s) and ultraluminous X-ray sources (ULXs) offers other intriguing hints. In some local NLS1s, the models of optical/UV accretion-disc emission overpredict the observed X-ray spectrum, suggesting that a large fraction of the accretion power is not converted into radiation but employed to launch a wind (Jin et al. 2017). Similarly, it has been recently proposed that

the so-called ultraluminous supersoft sources, arguably the most exotic class of accreting objects, are simply ULXs seen through an optically thick wind (Urquhart & Soria 2016). This sheds new light also on the X-ray weakness of quasars, which might be at the same time a requisite for winds (for instance, by avoiding over-ionization and so enabling line driving; Murray et al. 1995) and their consequence. If the broadband spectral energy distribution retains the signatures of the blow-out phase, X-ray winds can be studied even when the usual Fe K tracers are inaccessible. This is of primary importance for the prospect of extending the 'momentum boost' diagram to the high-redshift AGN populations around the peak of the cosmic accretion history, when winds must have shaped the galaxies as we see them today.

These and other relevant aspects of AGN outflows will be investigated in more detail from both an observational and a theoretical standpoint in future works.

ACKNOWLEDGMENTS

We thank the anonymous referee for the insightful and constructive comments that helped us improve the clarity of the paper, and Chiara Feruglio, Nozomu Kawakatu, Eleonora Sani, Francesco Tombesi and XianZhong Zheng for sharing information or useful discussion. EN acknowledges funding from the European Union's Horizon 2020 research and innovation programme under the Marie Skłodowska-Curie grant agreement no. 664931, and is grateful to the Centre for Extragalactic Astronomy, Durham University, for recurrent hospitality. KZ is funded by the Research Council Lithuania through the grant no. MIP-17-78.

REFERENCES

Aalto S., et al., 2015, A&A, 574, A85
Bentz M. C., et al., 2013, ApJ, 767, 149
Bae H.-J., Woo J.-H., Karouzos M., Gallo E., Flohic H., Shen Y., Yoon S.-J., 2017, ApJ, 837, 91
Bischetti M., et al., 2017, A&A, 598, A122
Capelo P. R., Volonteri M., Dotti M., Bellovary J. M., Mayer L., Governato F., 2015, MNRAS, 447, 2123
Carniani S., et al., 2015, A&A, 580, A102
Cicone C., et al., 2014, A&A, 562, A21
Cicone C., Brusa M., Ramos Almeida C., Cresci G., Husemann B., Mainieri V., 2018, NatAs, 2, 176
Ciotti L., Ostriker J. P., 1997, ApJ, 487, L105
Ciotti L., Ostriker J. P., 2001, ApJ, 551, 131
Crenshaw D. M., Kraemer S. B., 2012, ApJ, 753, 75
Dasyra K. M., et al., 2006, ApJ, 651, 835
Downes D., Solomon P. M., 1998, ApJ, 507, 615
Dunn J. P., et al., 2010, ApJ, 709, 611
Fabian A. C., 2012, ARA&A, 50, 455
Faucher-Giguère C.-A., Quataert E., 2012, MNRAS, 425, 605
Feruglio C., Maiolino R., Piconcelli E., Menci N., Aussel H., Lamastra A., Fiore F., 2010, A&A, 518, L155
Feruglio C., et al., 2015, A&A, 583, A99
Fiore F., et al., 2017, A&A, 601, A143
Fischer J., et al., 2010, A&A, 518, L41
Gabor J. M., Bournaud F., 2014, MNRAS, 441, 1615
Gibson R. R., et al., 2009, ApJ, 692, 758
Gofford J., Reeves J. N., Tombesi F., Braito V., Turner T. J., Miller L., Cappi M., 2013, MNRAS, 430, 60
González-Alfonso E., et al., 2014, A&A, 561, A27
González-Alfonso E., et al., 2017, ApJ, 836, 11
Hamann F., Chartas G., Reeves J., Nardini E., 2018, MNRAS, in press
Hao C. N., Xia X. Y., Mao S., Wu H., Deng Z. G., 2005, ApJ, 625, 78
Hagino K., Odaka H., Done C., Tomaru R., Watanabe S., Takahashi T., 2016, MNRAS, 461, 3954
Harrison C. M., 2017, NatAs, 1, 0165
Harrison C. M., Alexander D. M., Mullaney J. R., Swinbank A. M., 2014, MNRAS, 441, 3306
Harrison C. M., Costa T., Tadhunter C. N., Flütsch A., Kakkad D., Perna M., Vietri G., 2018, NatAs, 2, 198
Ishibashi W., Fabian A. C., Maiolino R., 2018, MNRAS, 476, 512
Jin C., Done C., Ward M., Gardner E., 2017, MNRAS, 471, 706
Kawakatu N., Imanishi M., Nagao T., 2007, ApJ, 661, 660
King A., 2003, ApJ, 596, L27
King A. R., 2010, MNRAS, 402, 1516
King A., Nixon C., 2015, MNRAS, 453, L46
King A., Pounds K., 2015, ARA&A, 53, 115
King A. R., Zubovas K., Power C., 2011, MNRAS, 415, L6
Kormendy J., Ho L. C., 2013, ARA&A, 51, 511
Krongold Y., Nicastro F., Elvis M., Brickhouse N., Binette L., Mathur S., Jiménez-Bailón E., 2007, ApJ, 659, 1022
Landt H., Ward M. J., Peterson B. M., Bentz M. C., Elvis M., Korista K. T., Karovska M., 2013, MNRAS, 432, 113
Leighly K. M., Terndrup D. M., Baron E., Lucy A. B., Dietrich M., Gallagher S. C., 2014, ApJ, 788, 123
Lípari S., Terlevich R., Díaz R. J., Taniguchi Y., Zheng W., Tsvetanov Z., Carranza G., Dottori H., 2003, MNRAS, 340, 289
Lipari S., et al., 2009, MNRAS, 392, 1295
Liu G., Zakamska N. L., Greene J. E., Nesvadba N. P. H., Liu X., 2013, MNRAS, 436, 2576
Luo B., et al., 2014, ApJ, 794, 70
Maiolino R., et al., 2012, MNRAS, 425, L66
Maiolino R., et al., 2017, Natur, 544, 202
Morganti R., Veilleux S., Oosterloo T., Teng S. H., Rupke D., 2016, A&A, 593, A30
Murray N., Chiang J., Grossman S. A., Voit G. M., 1995, ApJ, 451, 498
Nardini E., Risaliti G., Watabe Y., Salvati M., Sani E., 2010, MNRAS, 405, 2505
Nardini E., et al., 2015, Sci, 347, 860
Nayakshin S., Power C., King A. R., 2012, ApJ, 753, 15
Parker M. L., et al., 2017, Natur, 543, 83
Pinto C., Middleton M. J., Fabian A. C., 2016, Natur, 533, 64
Reynolds C. S., 2012, ApJ, 759, L15
Richings A. J., Faucher-Giguère C.-A., 2017, arXiv, arXiv:1710.09433
Rosario D. J., et al., 2018, MNRAS, 473, 5658
Rothberg B., Fischer J., Rodrigues M., Sanders D. B., 2013, ApJ, 767, 72
Rupke D. S. N., Veilleux S., 2011, ApJ, 729, L27
Rupke D. S. N., Veilleux S., 2013, ApJ, 768, 75
Rupke D. S. N., Gültekin K., Veilleux S., 2017, ApJ, 850, 40
Rupke D. S., Veilleux S., Sanders D. B., 2005, ApJ, 632, 751
Schawinski K., Koss M., Berney S., Sartori L. F., 2015, MNRAS, 451, 2517
Spoon H. W. W., Holt J., 2009, ApJ, 702, L42
Sturm E., et al., 2011, ApJ, 733, L16
Tacchella S., et al., 2015, Sci, 348, 314
Takeuchi S., Ohsuga K., Mineshige S., 2013, PASJ, 65, 88
Teng S. H., et al., 2014, ApJ, 785, 19
Tombesi F., Cappi M., Reeves J. N., Palumbo G. G. C., Yaqoob T., Braito V., Dadina M., 2010, A&A, 521, A57
Tombesi F., Meléndez M., Veilleux S., Reeves J. N., González-Alfonso E., Reynolds C. S., 2015, Natur, 519, 436
Tombesi F., Veilleux S., Meléndez M., Lohfink A., Reeves J. N., Piconcelli E., Fiore F., Feruglio C., 2017, ApJ, 850, 151

Urquhart R., Soria R., 2016, MNRAS, 456, 1859
Veilleux S., et al., 2009a, ApJ, 701, 587
Veilleux S., et al., 2009b, ApJS, 182, 628–666
Veilleux S., et al., 2013a, ApJ, 764, 15
Veilleux S., et al., 2013b, ApJ, 776, 27
Veilleux S., Meléndez M., Tripp T. M., Hamann F., Rupke D. S. N., 2016, ApJ, 825, 42
Veilleux S., Bolatto A., Tombesi F., Meléndez M., Sturm E., González-Alfonso E., Fischer J., Rupke D. S. N., 2017, ApJ, 843, 18
Zheng X. Z., Xia X. Y., Mao S., Wu H., Deng Z. G., 2002, AJ, 124, 18
Zubovas K., 2018, MNRAS, 473, 3525
Zubovas K., King A., 2012, ApJ, 745, L34
Zubovas K., King A. R., 2014, MNRAS, 439, 400
Zubovas K., King A., 2016, MNRAS, 462, 4055